Slower shortening kinetics of cardiac muscle performing Windkessel work-loops increases mechanical efficiency

Amy S. Garrett[1*], Denis S. Loiselle[1,2], Andrew J. Taberner[1,3], June-Chiew Han[1]

[1] Auckland Bioengineering Institute, The University of Auckland, New Zealand

[2] Department of Physiology, The University of Auckland, New Zealand

[3] Department of Engineering Science, The University of Auckland, New Zealand

Running Title: Energetics of model-loaded heart muscle

Key words: Cardiac muscle, Work-loop, Efficiency, Mechano-energetics, Windkessel

* Correspondence:

Amy Garrett

ORCID: 0000-0002-7176-0918

Auckland Bioengineering Institute

70 Symonds Street, Auckland, New Zealand

amy.garrett@auckland.ac.nz

Downloaded from journals.physiology.org/journal/ajpheart at Univ of Auckland Lib (130.216.209.065) on August 2, 2022.

New and Noteworthy

Cardiac muscle samples were allowed to describe their natural shortening dynamics while performing force length work and liberating heat. The muscle shortened more slowly and produced greater force and work output against a time-varying 'Windkessel' load than during conventional constant-force shortening, thereby yielding greater mechanical efficiency. A key finding is that the slower shortening kinetics developed in the face of a time-varying load enhances the mechanical efficiency of cardiac muscle during work-loop contractions.

Downloaded from journals.physiology.org/journal/ajpheart at Univ of Auckland Lib (130.216.209.065) on August 2, 2022.

Abstract

Conventional experimental methods for studying cardiac muscle *in vitro* often do not expose the tissue preparations to a mechanical impedance that resembles the *in vivo* hemodynamic impedance dictated by the arterial system. That is, the afterload in work-loop contraction is conventionally simplified to be constant throughout muscle shortening, and at a magnitude arbitrarily defined. This conventional afterload does not capture the time-varying interaction between the left ventricle and the arterial system. We have developed a contraction protocol for isolated tissue experiments that allows the afterload to be described within a Windkessel framework that captures the mechanics of the large arteries. We aim to compare the energy expenditure of cardiac muscle undergoing the two contraction protocols: conventional versus Windkessel loading. Isolated rat left-ventricular trabeculae were subjected to the two force-length work-loop contractions. Mechanical work and heat liberation were assessed, and mechanical efficiency quantified, over wide ranges of afterloads or peripheral resistances. Both extent of shortening and heat output were unchanged between protocols, but peak shortening velocity was 39.0 % lower and peak work output was 21.8 % greater when muscles contracted against the Windkessel afterload than against the conventional isotonic afterload. The greater work led to a 25.2 % greater mechanical efficiency. Our findings demonstrate that the mechanoenergetic performance of cardiac muscles *in vitro* may have been previously constrained by the conventional, arbitrary, loading method. A Windkessel loading protocol, by contrast, unleashes more cardiac muscle mechanoenergetic potential, where the slower shortening increases efficiency in performing mechanical work.

Downloaded from journals.physiology.org/journal/ajpheart at Univ of Auckland Lib (130.216.209.065) on August 2, 2022.

Introduction

Beat-by-beat ventricular contraction is characterised by pressure-volume loops consisting of four sequential phases: isovolumic contraction, ventricular (after-loaded) ejection, isovolumic relaxation and diastolic refilling. The ventricular ejection phase, including its transition from and to its adjacent phases, is of particular interest as its mechanics are closely coupled to the dynamics of the arterial system. The characteristic impedance and compliance of the large arteries, and the downstream resistance of the peripheral arterial systems, affect the extent and timing of pressure developed by the ventricles. The energy stored during systole in the large elastic arteries is then dissipated by the blood throughout the arterial system during diastole This coupling between the ventricle and the arterial system was first described by Frank (1) (translated into English by Sagawa et al. (2)) with the use of a 2-element Windkessel model comprising an arterial compliance (C) and a peripheral resistance (R_P). This 2-element model was later expanded to include a third element in order to capture the characteristic aortic impedance (Z_C) (3, 4). The 3-element Windkessel model has since formed part of experimental or analytical protocols for the study of healthy left-ventricular (5-10) and right-ventricular (11-13) physiology. The 3-element Windkessel model has likewise be applied in diseased whole-hearts (14, 15).

When studying isolated muscle samples using trabeculae (16-18), papillary muscles (19-24) or individual cardiomyocytes (25-27), the force-length work-loops also consist of four sequential phases to resemble the pressure-volume loop *in vivo*: isometric contraction, afterloaded shortening, isometric relaxation and diastolic re-lengthening. The conventional method to achieve force-length work-loops involves controlling muscle length during the afterloaded shortening phase in order to maintain a constant value of force, arbitrarily chosen by the experimentalist. This simplified method results in 'flat-topped' force-length work-loops, mimicking an infinitely compliant vasculature once the afterload is reached. These loops do not fully reflect the dynamic, time-varying, nature of the ejection phase that is

Downloaded from journals.physiology.org/journal/ajpheart at Univ of Auckland Lib (130.216.209.065) on August 2, 2022.

modulated by ventricular-arterial coupling *in vivo*, typically exemplified by the dynamic, curved nature of the ejection trajectory of the pressure-volume loop. We hypothesise that a trabecula that is constrained to follow a 'flat-topped' shortening trajectory may not fully realise its potential to produce mechanical work, thereby failing to operate at its maximum energetic efficiency.

Loading protocols using 3-element Windkessel impedance loads have been adopted in isolated tissue experiments, using pre-calculated loads, to evaluate cardiac muscle mechanics (28-30). The current study extends the use of 3-element Windkessel impedance loads in isolated tissue experiments to encompass energetics by determining muscle energy efficiency from the ratio of work to the sum of work and active heat. Our model-based loading protocol incorporates a 3-element Windkessel model of vascular impedance (31, 32). This impedance, computed in real-time, rather than pre-calculated, gives rise to force-length shortening profiles that better mimic the dynamic pressure-volume ejection profiles. The current study compares cardiac mechano-energetic performance of isolated trabeculae between that which arises when contracting against a 3-element Windkessel model with that which arises when they are subjected to perform the conventional 'flat-topped' work-loops. Muscle mechano-energetic performance was assessed over a wide range of loads by varying the model parameter governing the arterial peripheral resistance.

Downloaded from journals.physiology.org/journal/ajpheart at Univ of Auckland Lib (130.216.209.065) on August 2, 2022.

Methods

The Work-Loop calorimeter

Experiments were conducted using a work-loop calorimeter (33-36). This device consists of a borosilicate glass measurement chamber (internal dimensions 1 mm square) inserted in a block of thermally conductive gold-plated copper. In each experiment, a trabecula was suspended between two platinum hooks in the measurement chamber and supplied with a constant flow of oxygen- and nutrient-rich Tyrode superfusate. Thermopile sensors mounted below and external to the measurement chamber generated a voltage proportional to the temperature increase of the superfusate as it flowed over the trabecula. The increased temperature of the superfusate was proportional to the rate of heat-release by the muscle.

A linear voice-coil motor, connected to the upstream hook, controlled muscle length. Muscle force development was measured using a cantilever-based force transducer connected to the downstream hook. Bending of the cantilever and the position of the linear motor were measured by a laser interferometer system. A LabVIEW RealTime and field-programmable gate array (FPGA) system houses the control architecture, which enables the performance of a range of contraction modes including isometric contractions (no shortening), and two shortening contractions: conventional constant-afterload ('flat-top') work-loops and Windkessel-loaded work-loops.

Conventional versus Windkessel work-loop loading

Isometric contractions, where muscle length was controlled to remain unchanged throughout a twitch, were achieved by compensating for the tiny deflection of the force transducer downstream with the upstream length-motor. In the conventional flat-top work-loop control mode, on elicitation of a muscle twitch, isometric force was allowed to develop to a user-selected, constant, afterload. The controller

Downloaded from journals.physiology.org/journal/ajpheart at Univ of Auckland Lib (130.216.209.065) on August 2, 2022.

123 then transitioned to isotonic mode, thereby allowing the muscle to shorten at that constant afterload
124 until the muscle could no longer sustain the afterload. At this point, the controller transitioned to
125 isometric mode to allow the muscle force to dissipate, whereupon the muscle was re-stretched to its
126 initial length.

127 A detailed description of our Windkessel loading technique has been published previously (31, 32).
128 Briefly, a 3-element Windkessel transfer function (Z_{WK}) was used to model the flow impedance
129 experienced by the left ventricle, dictated by the mechanics of the large arteries and peripheral arterial
130 system. The impedance transfer function of the model is as follows:

$$Z_{Wk}(s) = \frac{(Z_C R_P C)s + (Z_C + R_P)}{(R_P C)s + 1}$$

131 The impedance is equivalent to an electrical low-pass filter containing two resistors and a capacitor. In
132 this analogy, voltage and current are analogous to pressure and blood flow rate, respectively. The model
133 was parameterised by the characteristic aortic impedance (Z_C, Pa·s·m^{-3}), the arterial compliance
134 (C, m^3·Pa^{-1}) and the peripheral resistance (R_P, Pa·s·m^{-3}), the values of which were adapted from our
135 previous study (32). For any ventricular pressure, scaled from real-time measured muscle stress using
136 Laplace's Law, this impedance transfer function was used to predict, in real-time, a corresponding
137 ventricular outflow rate. The predicted outflow rate was then scaled using the dimensions of the
138 modelled ventricle, and used to control the rate of muscle shortening. The dimensions of this modelled
139 ventricle included a ventricular radius of 5 mm and a wall thickness of 2 mm, which were assumed
140 consistently across all experiments. Muscle re-stretch rate was the same as that used for the
141 conventional work-loop to provide consistency between protocols, where muscle length was returned
142 to L_o at a modelled 'flow rate' into the 'ventricle'. The model, encoded in a combination of software and
143 hardware, was computed at a rate of 20 kHz, and used to control muscle length throughout each twitch.

Downloaded from journals.physiology.org/journal/ajpheart at Univ of Auckland Lib (130.216.209.065) on August 2, 2022.

144

145

146 ***Experimental procedure***

147 Animal handling and euthanasia were performed in accordance with a protocol approved by The
148 University of Auckland's Animal Ethics committee (reference number 002006). Four male Wistar rats (10
149 weeks old, 250 g to 300 g) were used. Prior to euthanasia, each rat was injected with heparin (1000
150 IU kg^{-1}). Euthanasia was achieved via isoflurane (5 % in O_2) followed by cervical dislocation. The heart
151 was excised and immediately plunged into a chilled Tyrode solution. The aorta was cannulated and the
152 vasculature Langendorff-perfused with Tyrode solution at room temperature. The Tyrode perfusate
153 contained 130 mM NaCl, 6 mM KCl, 1 $MgCl_2$, 0.5 mM NaH_2PO_4, 10 mM HEPES, 10 mM glucose with
154 addition of 0.3 mM $CaCl_2$ and 20 mM 2,3-butanedione monoxime, and pH of 7.4 by using Tris.

155 The heart was opened along the septal boundary and trabeculae dissected from the left ventricle. A
156 suitably-sized trabecula was mounted onto hooks and advanced into the measurement chamber of the
157 calorimeter. Superfusate containing Tyrode solution and 1.5 mM $CaCl_2$ was supplied at a constant flow
158 rate of 0.55 µL/s. Contraction of the trabecula was induced via electrical field stimulation at a rate of
159 2 Hz. When muscle force had reached steady state, the muscle was stretched gradually to reach the
160 optimal length (L_o) to achieve maximal active force production. Muscle dimensions, including L_o and the
161 major and minor diameters, were measured using a microscope graticule. These dimensions were
162 utilised to inform the Windkessel model as well for post-experimental data processing. The entire
163 work-loop calorimeter was enclosed in an insulated chamber to minimise thermal fluctuations and
164 optical disturbances. The ambient temperature within the enclosure was maintained at 32 °C. The
165 combination of the rate of flow of superfusate, the rate of contraction, and temperature ensured
166 sufficient muscle oxygenation (37).

Downloaded from journals.physiology.org/journal/ajpheart at Univ of Auckland Lib (130.216.209.065) on August 2, 2022.

Experimental interventions

Each trabecula was presented with both the conventional 'flat-topped' work-loop and the Windkessel model-based work-loop protocols. Flat-topped work-loops were performed by applying a series of five-six loads at a constant force, ranging between the force at end diastole, and peak isometric force. A series of Windkessel work-loops was performed by decrementing the peripheral resistance term in six-seven steps from a 'high' impedance load (800 GPa.s.m^{-3}) to a 'low' impedance load ((30-50) GPa.s m^{-3}), interspersed with isometric contractions. The compliance and characteristic aortic impedance parameters were maintained constant across all muscles (C = 32 pm^3·Pa^{-1}, Z_c = 5 GPa·s·m^{-3}). The muscle was allowed to reach steady state under each work-loop and isometric contraction intervention. In order to obtain the isometric force-length relation, isometric contractions were performed at decrements of length in 5-6 steps until active force was no longer detectable. Muscle force and length were recorded throughout, simultaneous with muscle heat rate.

The recorded heat rate measured upon muscle contraction contained three components: active heat, change of basal heat, and electrical stimulus heat artefact. Hence, subsequent to the active contraction intervention, two additional interventions were required in order to accurately reveal the active heat output of the contracting muscle. Firstly, electrical stimulation was halted to allow muscle quiescence. The resting trabecula was then subjected to a series of length-change interventions to obtain data on the change of basal heat rate, which we have previously shown to be length- and velocity-dependent (38, 39). These data were needed, and post-experimentally processed, to compensate for the change of basal heat rate that occurs with a change of length, even in the presence of work production. Our model of basal heat rate provided a basal heat value for each afterload. Secondly, the heat artefact arising from electrical stimulation of the muscle was determined by measuring the heat signal in the measurement chamber with the mounting hooks in place, but in the absence of the muscle. The active heat rate was

Downloaded from journals.physiology.org/journal/ajpheart at Univ of Auckland Lib (130.216.209.065) on August 2, 2022.

revealed during each afterloaded work-loop contraction by subtracting from the measured heat rate signal the change of basal heat rate (at each afterload) and the stimulus heat artefact. The active heat rate at each afterload was quantified in relation to the neighbouring isometric periods, in order to account for implications of force rundown and potential temperature drift within the calorimeter enclosure.

Experimental design and muscle geometry

In total, n = 6 trabeculae isolated from four rat hearts were studied. Three were presented with the flat-topped work-loop intervention prior to the Windkessel work-loop intervention, while the other three received the converse order. Trabeculae, on average, had a minor diameter of 353 μm ± 20 μm (maximum 470 μm, minimum 235 μm), a major diameter of 390 μm ± 20 μm (maximum 470 μm, minimum 282 μm), and L_o of 3.24 mm ± 0.11 mm (maximum 3.95 mm, minimum 2.96 mm), giving an average cross-sectional area of 0.109 mm^2 ± 0.0099 mm^2 (maximum 0.17 mm^2, minimum 0.06 mm^2), and volume of 0.354 mm^3 ± 0.0357 mm^3 (maximum 3.95 mm^3, minimum 2.96 mm^3).

Data processing

Force was converted to stress by division with muscle cross-sectional area measured at L_o. Given that the data are paired where each muscle performed both contraction protocols, a single value of muscle cross-sectional area was used in this conversion. In the calculation of mechanical efficiency, as muscle cross-sectional area is common to both the numerator (i.e., mechanical work output) and the denominator (i.e., the sum of work and heat), efficiency is a dimensionless quantity.

The end systolic stress of each work loop was quantified by the velocity of shortening approaching zero (within a tolerance of 0.05 L/L_o per second). Thus, from a series of 5-6 afterloaded work-loops, a work-loop end systolic stress length relation was established by fitting to the 5-6 end systolic stresses. The

Downloaded from journals.physiology.org/journal/ajpheart at Univ of Auckland Lib (130.216.209.065) on August 2, 2022.

slope of the relation provides a measure of cardiac contractility. End systolic stress served as the independent variable for plotting against mechanoenergetic variables. Active stress was calculated as the end-systolic stress minus the passive stress at L_o for each set of work-loops. Muscle length was expressed relative to its optimal value (L/L_o). Work output was computed as the integral of developed stress with respect to length throughout a twitch, equivalent to the area of the stress-length work-loop. The extent of muscle shortening was given by the width of the work-loop. To calculate muscle heat rate, the thermopile voltage was corrected for stimulus heat and changes in basal heat, as described above, and then divided by the thermopile sensitivity (4000 V/W). Muscle heat per twitch was calculated by further division by the stimulus frequency (2 Hz). Mechanical efficiency was calculated as the ratio of work to the sum of work and active heat, where the denominator signifies the change of enthalpy.

Time to end-systole (top left corner of each work-loop) and time to end-contraction (bottom left corner of each work-loop) were determined based on the rate of change of length (i.e. velocity of shortening) and the rate of change of stress, respectfully, as they approached zero. The time difference between the stimulus pulse and when shortening velocity approached zero (within a tolerance of 0.05 L/L_o per second) determined the time to end-systole. The time difference between the stimulus pulse and when the rate of relaxation of the muscle approached zero, within a tolerance of 0.1 kPa per second determined the time to end-contraction.

Statistical Analyses

Data were plotted as functions of either the normalised end-systolic stress (with respect to isometric maxima), muscle length (relative to optimal length) or peripheral resistance (R_p). Data points were fitted using polynomial regression (up to third-order), and the regression lines were averaged within contraction type (flat-topped and Windkessel), and compared between the two loading types, using the Random Coefficient Model implemented in the SAS software package. Peak values of variables were

Downloaded from journals.physiology.org/journal/ajpheart at Univ of Auckland Lib (130.216.209.065) on August 2, 2022.

averaged and superimposed on the averaged regression lines, presented as mean ± standard error. Significant differences between peak values of variables were tested between contraction type using ANOVA implemented using the Proc Mixed model implemented in the SAS software package, where "Contraction Type" and "Order of presenting the Contraction Type" (i.e., whether Windkessel loading type was presented first or second) served as the Model statement, and "Muscle" served as a Random effect. Multiple comparisons were adjusted using Tukey's test. Statistical significance was declared when $p < 0.05$. In all comparisons, there were no statistical differences in the interaction effect of "Contraction Type" and "Order of presenting the Contraction Type". Hence, the Windkessel loading protocol presented first and the conventional loading protocol presented second were not different from the converse order.

Downloaded from journals.physiology.org/journal/ajpheart at Univ of Auckland Lib (130.216.209.065) on August 2, 2022.

Results

We compared flat-topped (conventional) versus Windkessel loading methods on cardiac muscle mechanoenergetics. For the conventional loading protocol, trabeculae were subjected to 6 different constant afterloads. For Windkessel loading, a series of Windkessel work-loops was performed by altering the peripheral resistance term in the Windkessel transfer function model. Figure 1 shows a typical experimental record of simultaneous measurement of twitch stress production and rate of active heat output from a representative trabecula, experiencing Windkessel loading. Rate of muscle active heat production (i.e., power) was calculated from the thermopile signal after first correcting for stimulus heat and changes in basal heat rate. Electrical stimulation commenced and the trabecula contracted isometrically until steady state (ISO), at which point the contraction mode was switched to 'work-loop' at a high afterload (labelled 'AF1'). Isometric contractions were performed, interspersed with work-loops at different afterloads. Heat rate decreased with decreasing afterload from 'AF1' (R_p = 800 GPa.s.m^{-3}) to 'AF6' (R_p = 50 Gpa.s.m^{-3}).

In Figure 2, parametric plots of the steady-state twitches and length change yielded stress-length work-loops. The Windkessel work-loops exemplified (Figure 2C) the effect of the dynamic nature of the model-based load. These 'curve-topped' loops each display a shortening trajectory that arises from the implementation of modelled loads while mimicking the effect of the ventricular-arterial coupling which arises *in vivo*. By comparison, the conventional work-loops were flat-topped, consequent to the constant-force loads (Figure 2F).

The difference in the work-loop profiles between the two types of loading was further exemplified when the flat-topped (red) and Windkessel-loaded (blue) loops were superimposed in Figure 3A. The end-systolic points of the work-loops were fitted by quadratic regression to obtain the work-loop end-systolic stress-length relations for both contraction modes (Figure 3B). In Figure 3C, the end-systolic

Downloaded from journals.physiology.org/journal/ajpheart at Univ of Auckland Lib (130.216.209.065) on August 2, 2022.

268 stress-length relations averaged from six trabeculae were not different between the Windkessel and the
269 conventional work-loop contractions. In addition, the relationship between end-systolic shortening
270 (shown as the percentage of L_o) and relative active end-systolic stress was not different between loading
271 types (figure 3C, insert) with a p-value of 0.0717. The *y*-intercept of these relationships, indicating the
272 peak extent of shortening, was also not different between loading types (*p*-value = 0.0970).

273 Closer examination of the shortening dynamics during loops at the lowest load, for the same muscle as
274 shown in Figure 3, provides a striking comparison, as shown in Figure 4. Although they may occasionally
275 occur coincidentally, work-loops with comparable shortening cannot be directly prescribed by the
276 experimentalist, as the afterload in Windkessel-loading arises from the peripheral resistance term, and
277 is not explicitly controlled. A coincidentally matched afterload is exemplified by the two work-loops
278 shown in Figure 4A-C, detailing the times at end-systole (annotated by triangles) and the times at
279 end-contraction (annotated by filled circles). Figure 4D and 4E displays both the time to end-systole and
280 the time to end-contraction, plotted as functions of end-systolic length normalised to L_o for a
281 representative muscle (panel D) and for the average of the six trabeculae (panel E). On average across
282 the six trabeculae, there was a significant difference in the time to end-systole ($p < 0.0001$) but with no
283 difference in the time to end-contraction ($p = 0.612$) between the two loading types (Figure 4E). These
284 results indicate that trabeculae under the Windkessel loading protocol shortened at a lower velocity
285 than under the conventional loading protocol (Figure 5). The average peak velocity of shortening was
286 2.56 s^{-1} ± 0.14 s^{-1} under the conventional loading but was 1.56 s^{-1} ± 0.13 s^{-1} under the Windkessel loading
287 (Figure 5B), representing a difference of 39.0 % ± 5.0 % (*p* = 0.00514). This slower shortening under the
288 Windkessel loading was followed by a faster relaxation, as indicated by the greater peak rate of stress
289 relaxation (Figure 4F-G) compared with the Windkessel loading ($p = 0.0004$).

290 The increased stress development during shortening of the Windkessel work-loops yielded a greater
291 work output, corresponding to the area of each work-loop. This result is revealed when work output is

Downloaded from journals.physiology.org/journal/ajpheart at Univ of Auckland Lib (130.216.209.065) on August 2, 2022.

plotted as a function of end-systolic stress in Figure 6A and B, where the peak value of work output was greater under the Windkessel work-loop contractions than under the conventional work-loop contractions (0.84 kJ/m^3 ± 0.09 kJ/m^3 versus 0.70 kJ/m^3 ± 0.1 kJ/m^3; p = 0.00422). Heat output and enthalpy output were not different between the two work-loop contraction protocols (Figure 6C and D). Consequently, mechanical efficiency, quantified as the ratio of work to enthalpy, was greater under the Windkessel work-loop contraction than under the conventional work-loop contractions (peak value 17.8 % ± 2.1 % versus 14.4 % ± 1.8 %; p = 0.0369; Figure 6F). Note that plotting both work and mechanical efficiency as functions of end-systolic strain (not shown) yielded the same conclusion: that both peak work and peak mechanical efficiency are greater under the Windkessel work-loop loading than under the conventional loading. This was consistent with the inherent correlation between shortening and active end-systolic stress (Figure 3C inset).

The relative end-systolic stress at which peak work occurred (namely the optimal end-systolic stress) was significantly lower under the Windkessel protocol than under the conventional work-loop contraction protocols (Figure 6B). The optimal relative end-systolic stress for peak work was 0.50 ± 0.02 under the Windkessel and 0.55 ± 0.03 under the conventional work-loop protocols (p = 0.0281). However, peak mechanical efficiency occurred at the optimal end-systolic stress (Figure 6F) of 0.41 ± 0.02 versus 0.45 ± 0.03 (p = 0.0610). These data are summarised in Figure 7 and expressed as fold-change, where the peak work was 21.8 % ± 4.7 % greater and the peak mechanical efficiency was 25.2 % ± 8.4 % greater under the Windkessel than under the conventional work-loop contractions. Figure 7E and F show, respectively, the work at peak efficiency (0.810 kJ/m^3 ± 0.088 kJ/m^3 versus 0.664 kJ/m^3 ± 0.096 kJ/m^3; p = 0.00429), and the heat at peak efficiency (4.06 kJ/m^3 ± 0.60 kJ/m^3 versus 4.14 kJ/m^3 ± 0.51 kJ/m^3; p = 0.730).

Figure 8 displays work, heat, enthalpy and mechanical efficiency as functions of peripheral resistance (R_p) for the Windkessel work-loop contractions. The optimal R_p for peak work and for peak mechanical

Downloaded from journals.physiology.org/journal/ajpheart at Univ of Auckland Lib (130.216.209.065) on August 2, 2022.

316 efficiency were interpolated from the curves and, have magnitudes of 174 GPa.s/m^3 ± 25 GPa.s/m^3 and

317 74 GPa.s/m^3 ± 20 GPa.s/m^3, respectively.

Downloaded from journals.physiology.org/journal/ajpheart at Univ of Auckland Lib (130.216.209.065) on August 2, 2022.

Discussion

In this study, we extend the use of the loading method based on a 3-element Windkessel model of the systemic arterial system to investigate cardiac mechanoenergetics in isolated trabeculae. By approximating, in real time, the arterial impedance experienced by the ventricle *in vivo*, an impedance load reflecting the haemodynamics of the arterial system is applied to cardiac muscle *in vitro*. This model-based loading allows, for the first time, evaluation of the effects of arterial haemodynamics on the mechanoenergetics of isolated trabeculae. Comparing the conventional and Windkessel loading methods, trabeculae *in vitro* liberated the same amount of active heat and underwent the same extent of shortening, over a wide range of afterloads prescribed by changing the model term governing peripheral resistance. However, with Windkessel loads, trabeculae developed greater stress during shortening, and shortened more slowly. Overall, with Windkessel loads, trabeculae accrued a 22 % increase in the peak work output, and, in consequence, contracted at a 25 % increase in peak mechanical efficiency.

Comparison to previous Windkessel-loading protocols: Loading methods using 3-element Windkessel impedance loads have been previously reported in whole-heart experiments (5-10) and in isolated tissue experiments (18, 29, 30). However, the applied loads have been either fluid-air systems, strictly applied to intact ventricles or have been pre-calculated, utilising physical electronic circuits or computational simulation offline. Moreover, in some of the previous studies, the resulting contraction was applied only to a single twitch, and not until steady state of force production upon a change of loading condition was achieved. In comparison, our real-time computation application in this study imposes fully-parameterised and real-time-computed loads to isolated cardiac tissues.

Selection of Windkessel parameters: Comparison between loading protocols required exploration of the full range of work-loops: from near zero to near peak isometric stress. Initial values for *C*

Downloaded from journals.physiology.org/journal/ajpheart at Univ of Auckland Lib (130.216.209.065) on August 2, 2022.

(compliance), Z_c (characteristic impedance) and R_p (peripheral resistance) were adapted from our previous study, where we have investigated the effects of each of the three model parameters, individually and the variation of all three in concert. In that previous study, we demonstrated that the effects of both C and Z_c were negligible in comparison with that of R_p alone in healthy muscles (32). Thus, in the present study to match the experimental conditions (32 °C and 2 Hz stimulation), we fixed the values of these parameters: C = 32 $pm^3 \cdot Pa^{-1}$ and Z_c = 5 $GPa \cdot s \cdot m^{-3}$, and varied the value of R_p from 50 $GPa \cdot s \cdot m^{-3}$ to 800 $GPa \cdot s \cdot m^{-3}$ (Figure 2). The selection of Windkessel parameters in the present study may lead to the incorrect perception that the end-systolic stress is 'identical' to the beginning stress required to transition from isometric contraction to afterloaded shortening in an work-loop (Figures 2C and 3A). But in this model configuration, the stress at the onset of shortening is always lower than the end-systolic stress. In our software, the modelled load dictates the onset, offset and profile of the shortening phase of the work-loop. These are determined by the pressure difference across the aortic valve in the modelled ventricle. It is only when the pressure developed in the 'ventricle' exceeds that which is stored and decaying in the aorta that the valve opens and ejection/shortening commences.

Windkessel loading increases efficiency: By applying our model-based loading method, we observed an average increase of 22 % in the peak work output. However, this increase in work was not accompanied by an increase in the heat output of the muscle, nor was the extent of shortening compromised. This indifference of heat to the dynamics of shortening indicates that, while the energy consumption of the contractile elements is dependent on load and extent of shortening, it is not dependent on the dynamics of the shortening achieved under these loads. The cross-bridges consume the same energy, liberate the same amount of heat, yet achieve more work. Given the same heat liberation but a greater mechanical work output, one might expect a greater change of enthalpy (the sum of work and heat). However, our data show no difference in the change of enthalpy between the two contraction protocols (Figure 6D). The reasons for this are: (i) that heat output is some 5-fold than work, and thus the

Downloaded from journals.physiology.org/journal/ajpheart at Univ of Auckland Lib (130.216.209.065) on August 2, 2022.

protocol-independent change of enthalpy in large part arises from the protocol-independent heat output; (ii) that peak work occurs at different optimal relative end-systolic stress, i.e., lower in the Windkessel loading (Figures 6B and 7B), and thus the protocol-independent change of enthalpy arises from different optimal relative end-systolic stresses of the quadratic function relating enthalpy to end-systolic stress (Figure 6D).

Protocol-independent heat output is not entirely surprising on two fronts. First, the two loading protocols result in the same total twitch duration where the time to end-contraction from the onset of contraction is the same. Second, they result in the same end-systolic stress-length relation (Figure 3C) and the same heat-stress relation (Figure 6D). The increase of work output for the same heat output provides a 25 % increase in the mechanical efficiency. This increased mechanical efficiency to a peak value of 18 % is closer to that measured from the working-heart (after accounting appropriately for basal oxygen consumption) - 21 % (40). The lower efficiency arising during the conventional loading method implies that this protocol does not realise the full force-length work potential of the muscle, such that it is unnaturally constrained to operate at a lower efficiency. We discuss below that the greater efficiency from Windkessel loading reflects the higher force of shortening, which is achieved with a lower rate of shortening and affects the kinetics of relaxation.

Shortening characteristics: We evaluated muscle shortening during work-loop contractions using four distinct indices. The first index is the trajectory profile of shortening. As a consequence of the time-varying impedance predicted by the Windkessel model, and imposed on the muscle, shortening occurs along a trajectory that produces work-loops with curved shortening profiles (Figure 2). These dynamic shortening profiles resemble the pressure-volume ejection profiles exhibited by the ventricle observed *in vivo* (5, 6), which is unlike the conventional loading method that constraints the shortening trajectory to constant loads (‘flat-top’). The dynamic nature of the ejection curve *in vivo* arises from the mechanical coupling between the pressure-driving ventricle and the compliant downstream arterial

Downloaded from journals.physiology.org/journal/ajpheart at Univ of Auckland Lib (130.216.209.065) on August 2, 2022.

system. The large proximal arteries, acting as a filter, smooth out large ventricular cyclic pressure oscillations, thereby providing a more steady pressure source for the downstream arterial system (3). These ejection mechanics *in vivo* are replicated by isolated trabeculae under our Windkessel loading, as is evident in the resulting curved shortening trajectory.

The second index we used to characterise muscle shortening was its extent, taken as the width of each work-loop. Under the Windkessel loads, despite a dynamic, curved, shortening trajectory, the extent of shortening achieved is not different from that obtained under the conventional constant load. This reveals that the greater force developed during shortening under the Windkessel loading did not affect the extent of shortening. This behaviour yields the same end-systolic stress-length relations (Figure 3). Note that the end-systolic stress-length relations from the two work-loop contractions are different from those obtained from the isometric contraction (Figure 3), which is consistent with the concept of cardiac contraction mode-dependency (41, 42), which holds that a work-loop contraction that causes muscle shortening has its end-systolic point located below that of the isometric contraction.

The curved shortening trajectory, along with the same extent of shortening achieved in the Windkessel work-loop contraction versus the conventional work-loop contraction, prompts us to evaluate the time to reach end-systole. This third index for characterising muscle shortening reveals that trabeculae under Windkessel loading took longer to reach end-systole than when under the conventional loading (Figure 4). This finding suggests that the trabeculae shorten at a lower rate under the Windkessel loading. We therefore characterise muscle shortening by quantifying the velocity of shortening, and find, unsurprisingly, that this fourth index is indeed lower under Windkessel loading (Figure 5).

What is surprising to us, however, is that muscles shortening against the Windkessel load exhibit a different velocity-stress relation. We are aware that a different, lower, velocity-stress relation can be obtained at a lowered preload (42-44), at a reduced inotropic state (42), at a lower temperature (45), or

Downloaded from journals.physiology.org/journal/ajpheart at Univ of Auckland Lib (130.216.209.065) on August 2, 2022.

412 from muscles of different ventricular origin (46, 47), or those that have a larger proportion of the beta
413 isozyme comprising the myosin heavy chain (46, 48). Our experimental conditions meet none of these
414 criteria. We thus consider that it is solely the difference in the control schemes employed in the two
415 loading protocols that allows the difference in the position of the velocity-stress relations. Our thinking
416 is supported by a previous study (49) following our detailed scrutiny of their experimental records.
417 Although not explicitly quantified, their raw experimental data show that a lower velocity of shortening
418 immediately ensues upon an increase in load during the shortening phase of the work-loop twitch.
419 Whereas they employed the conventional loading protocol, which resulted in flat-top work-loops,
420 clamping of the load to increase the force at the early, medium, and late time-points during the
421 shortening phase all resulted in a decrease in the gradient of the length-time traces, suggesting a
422 decrease in the velocity of shortening. Hence, their results and ours demonstrate that different loadings
423 during the shortening phase affect the velocity of muscle shortening.

424 Taking all four indices together in characterising muscle shortening, we show that the Windkessel load,
425 owing to its dynamic nature, results in trabeculae developing greater force of shortening, over and
426 above that achieved under the conventional loading protocol. For Windkessel contractions, the
427 associated shortening is entirely dictated by the internal pressure states of the model, and is thus not
428 constrained by any pre-calculated trajectory. Greater force is associated with muscle shortening at a
429 lower rate, thereby spending more time during shortening and taking longer to reach end-systole. In
430 comparison, for the conventional 'flat-top' loading protocol, the muscle shortens more rapidly,
431 compensating for force development and resulting in a flat-top shortening profile.

432 From this study, our new finding is focussed on the energetics and efficiency of contractions. The
433 temporal profile of shortening (or ejection) affects force (pressure) has been observed in several whole–
434 heart study, including those by Hunter et al. (50, 51). Our findings demonstrate that the dependence of
435 the mechanical property on the temporal profile during shortening is intrinsic to muscle tissues, and that

Downloaded from journals.physiology.org/journal/ajpheart at Univ of Auckland Lib (130.216.209.065) on August 2, 2022.

436 it affects mechanical efficiency. Hunter et al. (50, 51) concluded that the “larger changes in pressure”
437 early in systole is attributed to the dominant effect of the ‘elasticity’ component, and this effect
438 progressively diminishes later in systole. In contrast, the contribution of the ‘resistive’ component
439 progressively increases from early to late systole. Our observation that Windkessel work-loops develop a
440 greater force of shortening than Conventional work-loops early in systole may confirm a dominant effect
441 of the ‘elasticity’ component, as proffered by Hunter et al. (50, 51).

442 **Relaxation characteristics:** An interesting characteristic was obtained during the relaxation phase of the
443 work-loop. The total time to end-contraction from onset of contraction remains unchanged despite the
444 two distinct loading protocols affecting the time to end-systole (Figure 4). Thus, the slower shortening
445 phase induced by the Windkessel loading is followed by a faster isometric relaxation phase than for the
446 conventional loading, as quantified by the rate of twitch relaxation (d*S*/d*t*; Figure 4F-G), resulting in no
447 difference in the time to end-contraction from the onset of contraction. The faster isometric relaxation
448 phase does not appear to be a consequence of the difference in the timing of re-stretch of the two
449 loading schemes, where the conventional loading re-stretches muscle immediately after complete
450 relaxation, whereas the Windkessel loading allows the muscle to remain at end-systolic length for a
451 longer period of time (Figure 4B). Note that under each of the two loading protocols, the rate of muscle
452 re-stretch, dictated by a constant filling flow rate to the ‘ventricle’ in the model, is the same for both
453 loading protocols. In both cases, we have allowed the muscle to relax fully prior to re-stretching. The
454 rate of re-stretch could be modelled in a future study, which would include the addition of the
455 pulmonary arterial impedance to our systemic arterial impedance in order to provide a model-based
456 estimate of preload. Given that both loading protocols re-stretch the relaxed muscle at the same rate,
457 the influence of the re-stretch phase on the area of each work-loop, and on the net work done is
458 identical between protocols.

Downloaded from journals.physiology.org/journal/ajpheart at Univ of Auckland Lib (130.216.209.065) on August 2, 2022.

459 The faster relaxation under Windkessel loading seems to be a consequence of the higher force
460 development during shortening. We are aware of studies demonstrating that cardiac muscle relaxation
461 is sensitive to load. In our experiments, each muscle underwent isometric relaxation, consistently
462 independent of loading protocol. In contrast, isotonic relaxation can be achieved by fully re-lengthening
463 muscle following end-systole, i.e., stretching of the muscle back to its initial length before complete
464 relaxation. The resultant work-loop twitch has a prolonged 'flat-top' region given the re-lengthening to
465 maintain the constant afterload following end-systole. This isotonic relaxation method directly modifies
466 the relaxation pattern to demonstrate that a stretch is necessary to accelerate relaxation (52-55).
467 Isotonic relaxation can also be achieved by re-stretching the muscle at variable rates following
468 end-systole. Such isotonic relaxation also directly modifies the relaxation pattern and reveals that
469 myocardial relaxation is sensitive to strain rate (56, 57). The consistent finding from these isotonic
470 relaxation methods is that a delayed end-systole accelerates relaxation. Our results, from isometric
471 relaxation, are in agreement that the delayed end-systole under the Windkessel loading accelerates
472 relaxation. These data illustrate the sensitivity of muscle relaxation to load, and support our assertion
473 that the faster relaxation under the Windkessel loading accompanies higher force production during
474 shortening.

475 **A link to the whole-heart:** By computing and applying a dynamic afterload based on a Windkessel
476 model, parameterised by measurable biophysical properties of the arterial system and
477 ventricular-arterial coupling, the effects of changing model parameters can now be explored. Here, we
478 demonstrate the effect of varying the peripheral resistance term (R_p) in the modelled load to perform a
479 wide range of work loops, where the work and efficiency can now be expressed as functions of this
480 model parameter (Figure 8). The resulting relationships exhibit a relatively sharp peak at low values of
481 R_p, that decays with increasing R_p, aligning with those observed in whole-heart impedance loading
482 experiments (5, 6, 58-63). Plotting measured mechanoenergetic variables in the whole-heart studies

Downloaded from journals.physiology.org/journal/ajpheart at Univ of Auckland Lib (130.216.209.065) on August 2, 2022.

have allowed understanding of the interaction and matching between the left ventricle and the arterial impedance load. Our experimental approach now allows *in vitro* investigation of the ways in which arterial impedance parameters affect muscle work output and efficiency, while bridging the gap between muscle and whole-heart experiments.

Conclusion

In conclusion, this study reveals that isolated trabeculae, when impeded by a load modelled on *in vivo* arterial haemodynamics, realise more of their stress-length work potential, with resulting increased mechanical efficiency. By contrast, the conventional 'flat-top' work-loop protocol may have restricted the work produced by the muscle, therefore constraining the muscle to operate at a lower efficiency. The increased mechanical efficiency is achieved directly from the increased force during shortening at a lower velocity without a change in the extent of shortening or heat production.

Downloaded from journals.physiology.org/journal/ajpheart at Univ of Auckland Lib (130.216.209.065) on August 2, 2022.

References

1. **Frank O**. Die Grundform des arteriellen Pulses. *Z Biol-Munich* 37: 1899.
2. **Sagawa K, Lie RK, and Schaefer J**. Translation of Otto Frank's paper "Die Grundform des Arteriellen Pulses" Zeitschrift fur Biologie 37: 483-526 (1899). *J Mol Cell Cardiol* 22: 253-254, 1990.
3. **Westerhof N, Lankhaar JW, and Westerhof BE**. The arterial Windkessel. *Med Biol Eng Comput* 47: 131-141, 2009.
4. **Westerhof N, Bosman F, De Vries CJ, and Noordergraaf A**. Analog studies of the human systemic arterial tree. *J Biomech* 2: 121-143, 1969.
5. **De Tombe PP, Jones S, Burkhoff D, Hunter WC, and Kass DA**. Ventricular stroke work and efficiency both remain nearly optimal despite altered vascular loading. *Am J Physiol* 264: H1817-1824, 1993.
6. **Sunagawa K, Maughan WL, and Sagawa K**. Optimal arterial resistance for the maximal stroke work studied in isolated canine left ventricle. *Circ Res* 56: 586-595, 1985.
7. **Suga H, and Sagawa K**. End-diastolic and end-systolic ventricular volume clamper for isolated canine heart. *Am J Physiol* 233: H718-722, 1977.
8. **Maughan WL, Sunagawa K, and Sagawa K**. Effects of arterial input impedance on mean ventricular pressure-flow relation. *Am J Physiol* 247: H978-983, 1984.
9. **Midei MG, Maughan WL, Oikawa RY, Kass DA, and Sagawa K**. Extracardiac pressure changes do not alter contractile function of the isolated left ventricle. *Ann Biomed Eng* 15: 347-359, 1987.
10. **Elzinga G, and Westerhof N**. Pump function of the feline left heart: changes with heart rate and its bearing on the energy balance. *Cardiovasc Res* 14: 81-92, 1980.
11. **Lankhaar JW, Westerhof N, Faes TJ, Marques KM, Marcus JT, Postmus PE, and Vonk-Noordegraaf A**. Quantification of right ventricular afterload in patients with and without pulmonary hypertension. *Am J Physiol Heart Circ Physiol* 291: H1731-1737, 2006.
12. **Chemla D, Lau EM, Papelier Y, Attal P, and Herve P**. Pulmonary vascular resistance and compliance relationship in pulmonary hypertension. *Eur Respir J* 46: 1178-1189, 2015.
13. **Saouti N, Westerhof N, Postmus PE, and Vonk-Noordegraaf A**. The arterial load in pulmonary hypertension. *Eur Respir Rev* 19: 197-203, 2010.
14. **Sunagawa K, Maughan WL, Burkhoff D, and Sagawa K**. Left ventricular interaction with arterial load studied in isolated canine ventricle. *Am J Physiol* 245: H773-780, 1983.
15. **Fukumitsu M, Kawada T, Shimizu S, Turner MJ, Uemura K, and Sugimachi M**. Development of a servo pump system for in vivo loading of pathological pulmonary artery impedance on the right ventricle of normal rats. *Am J Physiol Heart Circ Physiol* 310: H973-983, 2016.
16. **Han JC, Taberner AJ, Nielsen PM, Kirton RS, Ward ML, and Loiselle DS**. Energetics of stress production in isolated cardiac trabeculae from the rat. *Am J Physiol Heart Circ Physiol* 299: H1382-1394, 2010.
17. **Taberner AJ, Han JC, Kirton RS, Loiselle DS, and Nielsen PM**. Stress development, heat production and dynamic modulus of rat isolated cardiac trabeculae revealed in a flow-through micro-mechano-calorimeter. *Conf Proc IEEE Eng Med Biol Soc* 2010: 1860-1863, 2010.
18. **Han JC, Tran K, Crossman DJ, Curl CL, Koutsifeli P, Neale JPH, Li X, Harrap SB, Taberner AJ, Delbridge LMD, Loiselle DS, and Mellor KM**. Cardiac mechanical efficiency is preserved in primary cardiac hypertrophy despite impaired mechanical function. *J Gen Physiol* 153: 2021.
19. **Mellors LJ, and Barclay CJ**. The energetics of rat papillary muscles undergoing realistic strain patterns. *J Exp Biol* 204: 3765-3777, 2001.

Downloaded from journals.physiology.org/journal/ajpheart at Univ of Auckland Lib (130.216.209.065) on August 2, 2022.

538 20. **Mellors LJ, Gibbs CL, and Barclay CJ**. Comparison of the efficiency of rat papillary muscles during
539 afterloaded isotonic contractions and contractions with sinusoidal length changes. *J Exp Biol* 204: 1765-
540 1774, 2001.
541 21. **Barclay CJ, Widen C, and Mellors LJ**. Initial mechanical efficiency of isolated cardiac muscle. *J*
542 *Exp Biol* 206: 2725-2732, 2003.
543 22. **Hisano R, and Cooper Gt**. Correlation of force-length area with oxygen consumption in ferret
544 papillary muscle. *Circ Res* 61: 318-328, 1987.
545 23. **Layland J, Young IS, and Altringham JD**. The length dependence of work production in rat
546 papillary muscles in vitro. *J Exp Biol* 198: 2491-2499, 1995.
547 24. **Sorhus V, Sys SU, Natans A, Demolder MJ, and Angelsen BA**. Controlled auxotonic twitch in
548 papillary muscle: a new computer-based control approach. *Comput Biomed Res* 33: 398-415, 2000.
549 25. **Iribe G, Helmes M, and Kohl P**. Force-length relations in isolated intact cardiomyocytes
550 subjected to dynamic changes in mechanical load. *Am J Physiol Heart Circ Physiol* 292: H1487-1497,
551 2007.
552 26. **Iribe G, Kaneko T, Yamaguchi Y, and Naruse K**. Load dependency in force-length relations in
553 isolated single cardiomyocytes. *Prog Biophys Mol Biol* 115: 103-114, 2014.
554 27. **Helmes M, Najafi A, Palmer BM, Breel E, Rijnveld N, Iannuzzi D, and van der Velden J**.
555 Mimicking the cardiac cycle in intact cardiomyocytes using diastolic and systolic force clamps; measuring
556 power output. *Cardiovasc Res* 111: 66-73, 2016.
557 28. **Elzinga G, and Westerhof N**. "Pressure-volume" relations in isolated cat trabecula. *Circ Res* 49:
558 388-394, 1981.
559 29. **Elzinga G, and Westerhof N**. Isolated cat trabeculae in a simulated feline heart and arterial
560 system. Contractile basis of cardiac pump function. *Circ Res* 51: 430-438, 1982.
561 30. **de Tombe PP, and Little WC**. Inotropic effects of ejection are myocardial properties. *Am J*
562 *Physiol* 266: H1202-1213, 1994.
563 31. **Garrett AS, Pham T, Loiselle DS, June-Chiew H, and Taberner AJ**. Real-time model-based control
564 of afterload for in vitro cardiac tissue experimentation. *Conf Proc IEEE Eng Med Biol Soc* 2017: 1287-
565 1290, 2017.
566 32. **Garrett AS, Pham T, Loiselle D, Han JC, and Taberner A**. Mechanical loading of isolated cardiac
567 muscle with a real-time computed Windkessel model of the vasculature impedance. *Physiol Rep* 7:
568 e14184, 2019.
569 33. **Taberner AJ, Hunter IW, Kirton RS, Nielsen PMF, and Loiselle DS**. Characterization of a flow-
570 through microcalorimeter for measuring the heat production of cardiac trabeculae. *Rev Sci Instrum* 76:
571 2005.
572 34. **Han JC, Taberner AJ, Kirton RS, Nielsen PM, Smith NP, and Loiselle DS**. A unique
573 micromechanocalorimeter for simultaneous measurement of heat rate and force production of cardiac
574 trabeculae carneae. *J Appl Physiol (1985)* 107: 946-951, 2009.
575 35. **Taberner AJ, Han JC, Loiselle DS, and Nielsen PM**. An innovative work-loop calorimeter for in
576 vitro measurement of the mechanics and energetics of working cardiac trabeculae. *J Appl Physiol (1985)*
577 111: 1798-1803, 2011.
578 36. **Taberner AJ, Han JC, Loiselle DS, and Nielsen PM**. A work-loop calorimeter for measuring the
579 force-length-heat relationship of working excised cardiac muscle fibers. *Conf Proc IEEE Eng Med Biol Soc*
580 2011: 1901-1904, 2011.
581 37. **Han JC, Taberner AJ, Kirton RS, Nielsen PM, Archer R, Kim N, and Loiselle DS**. Radius-
582 dependent decline of performance in isolated cardiac muscle does not reflect inadequacy of diffusive
583 oxygen supply. *Am J Physiol Heart Circ Physiol* 300: H1222-1236, 2011.

Downloaded from journals.physiology.org/journal/ajpheart at Univ of Auckland Lib (130.216.209.065) on August 2, 2022.

584 38. **Garrett AS, Loiselle DS, Han J-C, and Taberner AJ**. Compensating for changes in heart muscle
585 resting heat production in a microcalorimeter. In: *2020 42nd Annual International Conference of the IEEE*
586 *Engineering in Medicine & Biology Society (EMBC)*IEEE, 2020, p. 2557-2560.
587 39. **Garrett AS, Loiselle DS, Han J, and Taberner AJ**. Heat production in quiescent cardiac muscle is
588 length-, velocity-, and muscle-dependent: Implications for active heat measurement. *Exp Physiol* 2021.
589 40. **Han JC, Goo S, Barrett CJ, Mellor KM, Taberner AJ, and Loiselle DS**. The afterload-dependent
590 peak efficiency of the isolated working rat heart is unaffected by streptozotocin-induced diabetes.
591 *Cardiovasc Diabetol* 13: 4, 2014.
592 41. **Han JC, Pham T, Taberner AJ, Loiselle DS, and Tran K**. Solving a century-old conundrum
593 underlying cardiac force-length relations. *Am J Physiol Heart Circ Physiol* 316: H781-H793, 2019.
594 42. **Tran K, Taberner AJ, Loiselle DS, and Han JC**. Energetics Equivalent of the Cardiac Force-Length
595 End-Systolic Zone: Implications for Contractility and Economy of Contraction. *Frontiers in Physiology* 10:
596 2020.
597 43. **Gulch RW, and Jacob R**. Length-tension diagram and force-velocity relations of mammalian
598 cardiac muscle under steady-state conditions. *Pflugers Arch* 355: 331-346, 1975.
599 44. **Strauer BE**. Force-velocity relations of isotonic relaxation in mammalian heart muscle. *Am J*
600 *Physiol* 224: 431-434, 1973.
601 45. **de Tombe PP, and ter Keurs HE**. Force and velocity of sarcomere shortening in trabeculae from
602 rat heart. Effects of temperature. *Circ Res* 66: 1239-1254, 1990.
603 46. **Brooks WW, Bing OH, Blaustein AS, and Allen PD**. Comparison of contractile state and myosin
604 isozymes of rat right and left ventricular myocardium. *J Mol Cell Cardiol* 19: 433-440, 1987.
605 47. **Pham T, Han JC, Taberner A, and Loiselle D**. Do right-ventricular trabeculae gain energetic
606 advantage from having a greater velocity of shortening? *J Physiol* 595: 6477-6488, 2017.
607 48. **Han J-C, Tran K, Crossman DJ, Curl CL, Koutsifeli P, Neale JPH, Li X, Harrap SB, Taberner AJ,**
608 **Delbridge LMD, Loiselle DS, and Mellor KM**. Cardiac mechanical efficiency is preserved in primary
609 cardiac hypertrophy despite impaired mechanical function. *Journal of General Physiology* 153: 2021.
610 49. **Gillebert TC, Sys SU, and Brutsaert DL**. Influence of loading patterns on peak length-tension
611 relation and on relaxation in cardiac muscle. *J Am Coll Cardiol* 13: 483-490, 1989.
612 50. **Hunter WC, Janicki JS, Weber KT, and Noordergraaf A**. Flow-pulse response: a new method for
613 the characterization of ventricular mechanics. *Am J Physiol* 237: H282-292, 1979.
614 51. **Hunter WC, Janicki JS, Weber KT, and Noordergraaf A**. Systolic mechanical properties of the left
615 ventricle. Effects of volume and contractile state. *Circ Res* 52: 319-327, 1983.
616 52. **Brutsaert DL, Housmans PR, and Goethals MA**. Dual control of relaxation. Its role in the
617 ventricular function in the mammalian heart. *Circ Res* 47: 637-652, 1980.
618 53. **Goethals MA, Housmans PR, and Brutsaert DL**. Load-dependence of physiologically relaxing
619 cardiac muscle. *Eur Heart J* Suppl A: 81-87, 1980.
620 54. **Lecarpentier YC, Chuck LH, Housmans PR, De Clerck NM, and Brutsaert DL**. Nature of load
621 dependence of relaxation in cardiac muscle. *Am J Physiol* 237: H455-460, 1979.
622 55. **Brutsaert DL, and Sys SU**. Load Dependence of Relaxation. In: *Diastolic Relaxation of the Heart:*
623 *Basic Research and Current Applications for Clinical Cardiology*, edited by Grossman W, and Lorell BH.
624 Boston, MA: Springer US, 1988, p. 83-96.
625 56. **Chung CS, Hoopes CW, and Campbell KS**. Myocardial relaxation is accelerated by fast stretch,
626 not reduced afterload. *J Mol Cell Cardiol* 103: 65-73, 2017.
627 57. **Chung CS**. How myofilament strain and strain rate lead the dance of the cardiac cycle. *Arch*
628 *Biochem Biophys* 664: 62-67, 2019.
629 58. **Piene H, and Sund T**. Flow and power output of right ventricle facing load with variable input
630 impedance. *Am J Physiol* 237: H125-130, 1979.
631 59. **Piene H**. Impedance matching between ventricle and load. *Ann Biomed Eng* 12: 191-207, 1984.

Downloaded from journals.physiology.org/journal/ajpheart at Univ of Auckland Lib (130.216.209.065) on August 2, 2022.

60. **Elzinga G, and Westerhof N**. Matching between Ventricle and Arterial Load - an Evolutionary Process. *Circulation Research* 68: 1495-1500, 1991.
61. **Westerhof N, and Elzinga G**. The apparent source resistance of heart and muscle. *Ann Biomed Eng* 6: 16-32, 1978.
62. **van den Horn GJ, Westerhof N, and Elzinga G**. Interaction of heart and arterial system. *Ann Biomed Eng* 12: 151-162, 1984.
63. **van den Horn GJ, Westerhof N, and Elzinga G**. Optimal power generation by the left ventricle. A study in the anesthetized open thorax cat. *Circ Res* 56: 252-261, 1985.

Downloaded from journals.physiology.org/journal/ajpheart at Univ of Auckland Lib (130.216.209.065) on August 2, 2022.

Competing interests

All authors declare that they have no competing interests.

Data availability statement

The experimental data contributing to this study can be made available by the corresponding author upon request.

Author Contributions

Experiments, data analysis and initial manuscript drafting performed by AG. All authors contributed to the study design, data interpretation and final drafting and approval of manuscript.

Funding

The work was supported by a Doctoral Scholarship from The University of Auckland (awarded to AG), a Marsden Fast-Start grant (UOA1504) from the Royal Society of New Zealand (awarded to J-CH), a Sir Charles Hercus Health Research Fellowship (20/011) from the Health Research Council of New Zealand (awarded to J-CH), and a James Cook Research Fellowship from the Royal Society Te Apārangi (awarded to AT).

Acknowledgements

None.

Downloaded from journals.physiology.org/journal/ajpheart at Univ of Auckland Lib (130.216.209.065) on August 2, 2022.

Figure Legends

Figure 1: Simultaneous measurements of muscle stress and active heat rate. Data arose from a representative trabecula developing twitch stress (A) while liberating heat (B) upon 2-Hz electrical stimulation. Contraction mode alternated between isometric ('ISO') and Windkessel work-loop over six afterloads from a high impedance ('AF1', corresponding to a peripheral resistance of 800 GPa.s.m^{-3}) to a low impedance ('AF6', corresponding to a peripheral resistance of 50 GPa.s.m^{-3}). Within each contraction period, steady states of both twitch stress (A) and heat rate (B) were attained. A single twitch at steady state from each work-loop contraction period is shown in Figure 2A. Electrical stimulation was turned off at approximately 790 s and the muscle returned to quiescence.

Figure 2: Comparison of Windkessel work-loops and conventional work-loops. Comparison is made from single steady-state, overlaid, twitches on the stress-time plane (A and D) and on the length-time plane (B and E), where the parametric plots reveal the stress-length work-loops (C and F). The Windkessel work-loops were achieved by changing the parameter governing the peripheral resistance, thereby varying the afterload. The labels 'ISO' (isometric), 'AF1' (high afterload) and 'AF6' (low afterload) are consistent with those in Figure 1. The conventional work-loops were achieved simply by setting different constant stresses (static afterloads). At all six afterloads, the Windkessel work-loops each had a shortening trajectory that was time-varying whereas the conventional work-loops maintained constant force throughout the shortening profile.

Figure 3: Mechanics of Windkessel work-loop (blue) and conventional (flat-topped) work-loop (red) contractions. Stress and length are normalised to the peak values at optimal length (L_o). Data in A and B have been plotted from the same trabecula as in Figure 2. The average end-systolic stress regression lines from all 6 trabeculae are plotted in C. The stress-length work-loops in Panel A are the same data as in Figure 2C and 2F, but have been normalised to peak stress and superimposed to show differences between Windkessel loading (blue) and conventional loading (red). The black lines denote the isometric

Downloaded from journals.physiology.org/journal/ajpheart at Univ of Auckland Lib (130.216.209.065) on August 2, 2022.

683 total stress-length relation (top) and the isometric passive stress-length relation (bottom), fitted to the
684 data points using quadratic regression. The divisions of relative active end-systolic stress (ESS) and
685 relative ESS are indicated at the right of panel A. Both isometric stress-length relations (black) in Panel A
686 are reproduced in Panel B, along with the end-systolic points of the work-loop (red and blue points)
687 which have also been fitted using quadratic regression. The regression lines were averaged across all 6
688 trabeculae and are plotted in Panel C, where no statistical difference was detected between the
689 work-loop end-systolic relations arising from Windkessel loading and conventional loading. The insets
690 show the percentage of end-systolic shortening as a function of relative active ESS for the example
691 trabeculae (inset of panel B) and the average of 6 trabeculae (inset of panel C).

692 **Figure 4: Time-course of muscle shortening during work-loop contractions.** In Panels A-C, the data from
693 the lowest afterload in Figure 2 between Windkessel (blue) and conventional (red) loading protocols are
694 superimposed. The black open symbols indicate the time at end-systole (the end of muscle shortening),
695 whereas the shaded symbols indicate the time to end-contraction when active stress production had
696 ceased. Note that following isometric relaxation (at around 0.17 s; at the onset of the circles), the rate of
697 muscle re-stretch was controlled to be the same for the two loading protocols. In Panels D and E, the
698 two time-points (time to end-systole and time to end-contraction) were calculated for all afterloads for
699 an exemplar muscle (D) and for the average of all six muscles (E), plotted as functions of relative
700 end-systolic length (L_{ES}/L_o) and fitted with linear regression. Panels F and G are the peak rate of stress
701 relaxation (*dS/dt*) during this relaxation phase (between time to end-systole and time to end-
702 contraction) for an exemplar muscle (F) and for the average of all six muscles (G); data are fitted with
703 linear regression. In panels E and G, statistically significant difference between the regression lines from
704 Windkessel (blue) and conventional (red) loading type is indicated by the asterisk.

Downloaded from journals.physiology.org/journal/ajpheart at Univ of Auckland Lib (130.216.209.065) on August 2, 2022.

Figure 5: Velocity of shortening during Windkessel (blue, circles) and conventional (red, squares) work-loop contractions as functions of End-Systolic Stress. Data from a representative trabecula are shown in Panel A, and the average regression lines from all 6 trabeculae are plotted in Panel B. Velocity of shortening has been normalised to the optimal length (L_o) of trabeculae and plotted against active end-systolic stress (ESS) relative to the peak active stress at L_o. Velocity of shortening was computed from the twitch length profile (Figures 2B and 2E) as the maximal slope during the relaxation phase. Statistical significances between the peak velocity of shortening including the velocity-ESS regression lines from Windkessel (blue) and conventional (red) loading type is indicated by the asterisk. Panel C describes the fold-change for peak shortening velocity, displayed as means with standard errors normalised to the conventional loading (Conv.). Normalised peak velocity for each of the 6 trabeculae is paired between the two loading protocols (Conv: conventional; WK: Windkessel). The asterisk indicates a significantly lower peak velocity of shortening under the Windkessel loading in relation to that under the conventional loading.

Figure 6: Mechanical efficiency of Windkessel (blue, circles) and conventional (red, squares) work-loop contractions. Data from a representative trabecula are shown in the left Panels (A, C and E), and the average regression lines from all 6 trabeculae are plotted in the right Panels (B, D and F). Work was quantified by integrating twitch stress with respect to length throughout the time course of each work-loop twitch, which denotes the area within each work-loop in Figure 3. Enthalpy is the sum of work and heat. Mechanical efficiency is the ratio of work to enthalpy. Data points are fitted using linear regression for heat (broken lines C and D), quadratic regression for enthalpy (solid lines in C and D), and cubic regression, constrained at the origin, for both work (A and B) and efficiency (E and F). All regression lines are drawn to commence at relative passive stress (0.2 - 0.3), i.e. the ratio of passive stress to total stress (see Figure 3C). End-systolic stress (ESS) was normalised to the peak stress obtained under isometric contractions at L_o. Standard errors of means are superimposed at peak values for each

Downloaded from journals.physiology.org/journal/ajpheart at Univ of Auckland Lib (130.216.209.065) on August 2, 2022.

729 dependent variable. Differences between Windkessel (blue) and conventional (red) work-loop
730 contractions are declared for both peak work (B) and peak mechanical efficiency (F), as indicated by the
731 asterisks. The optimal end-systolic stress at which peak work occurred is significantly lower under the
732 Windkessel than the conventional work-loop contractions (0.50 ± 0.02 versus 0.55 ± 0.03 relative
733 end-systolic stress). However, the optimal end-systolic stress at which peak efficiency occurred is not
734 significantly different between loading protocols (0.41 ± 0.02 versus 0.45 ± 0.03 relative end-systolic
735 stress; $p = 0.0610$).

736 **Figure 7: Fold-change of mechano-energetic indices from conventional loading to Windkessel loading.**
737 In all panels, mechano-energetic indices (calculated from Figure 6) from the Windkessel (WK) loading
738 are normalised to those from the conventional (Conv.) loading. Data points are from all 6 muscles, each
739 paired between the two loading types. Bars indicate means ± standard errors. Differences between the
740 two loading types are indicated by an asterisk. Panels A and C display the peak values for work and
741 efficiency. Panels B and D show the optimal afterloads at which peak values for work and efficiency
742 occur. Panels E and F show the work and the heat at the optimal afterload at which peak efficiency
743 occurs. In panel D, the p-value for the difference in fold change is 0.0610.

744 **Figure 8: Energetics of Windkessel work-loop contractions as functions of peripheral resistance.** Data
745 from a representative trabecula are shown in the left panels (A, C and E), and the average regression
746 lines from all 6 trabeculae are plotted in the right panels (B, D and F). Work, heat, enthalpy, and
747 mechanical efficiency (defined as in Figure 6) are displayed as functions of peripheral resistance (R_P).
748 Each trabecula was subjected to the same range of peripheral resistance (R_p) and, hence, dependent
749 variables (and their means and standard errors) can be plotted as functions of the independent variable,
750 R_P. Data points are fitted using quadratic regression for enthalpy (C and D, solid lines), and for heat (C

Downloaded from journals.physiology.org/journal/ajpheart at Univ of Auckland Lib (130.216.209.065) on August 2, 2022.

751 and D, dashed lines) and cubic regression for both work (A and B) and efficiency (E and F). The blue error

752 bars in B and F are the interpolated peak values.

Downloaded from journals.physiology.org/journal/ajpheart at Univ of Auckland Lib (130.216.209.065) on August 2, 2022.

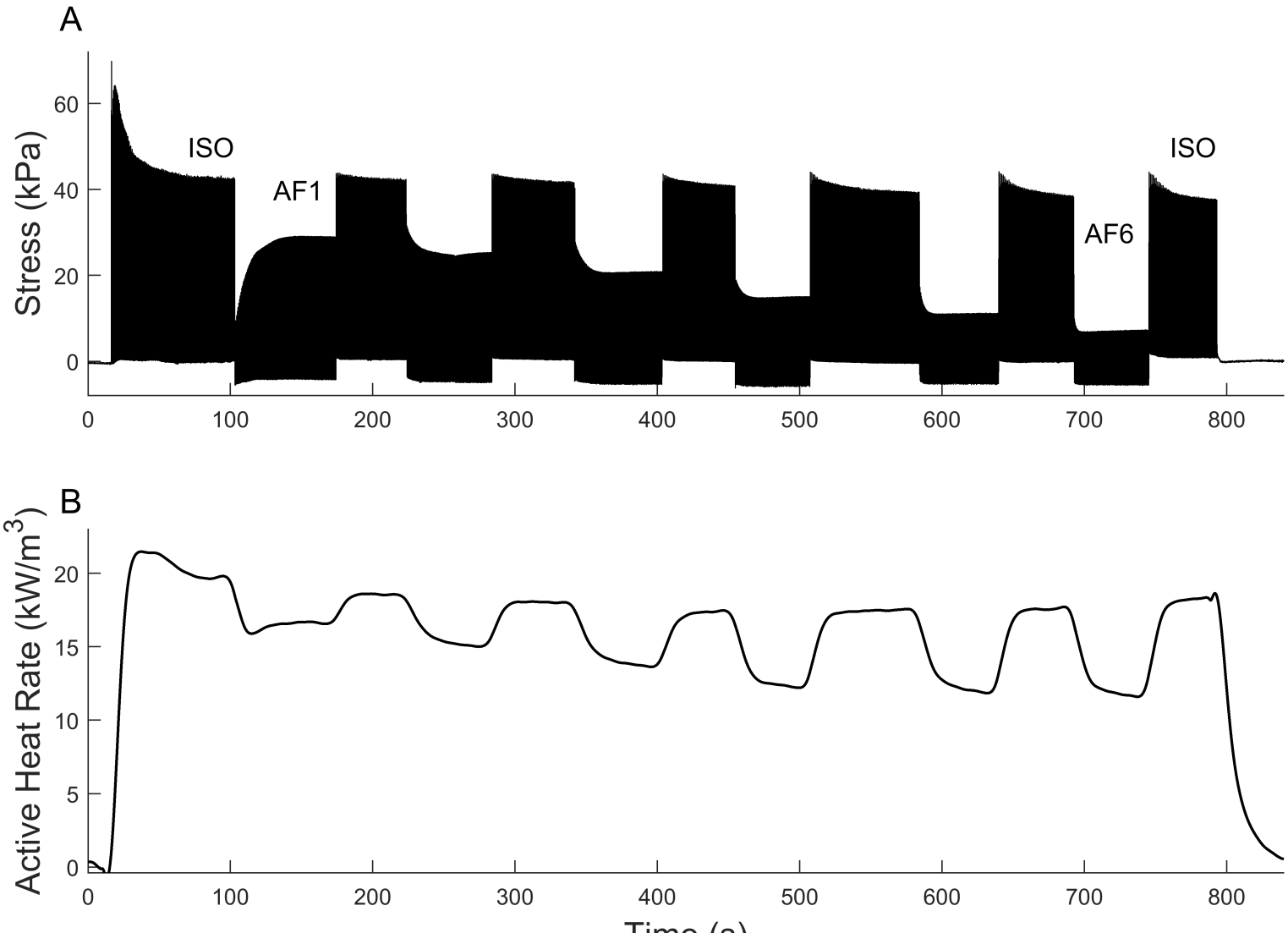

Downloaded from journals.physiology.org/journal/ajpheart at Univ of Auckland Lib (130.216.209.065) on August 2, 2022.

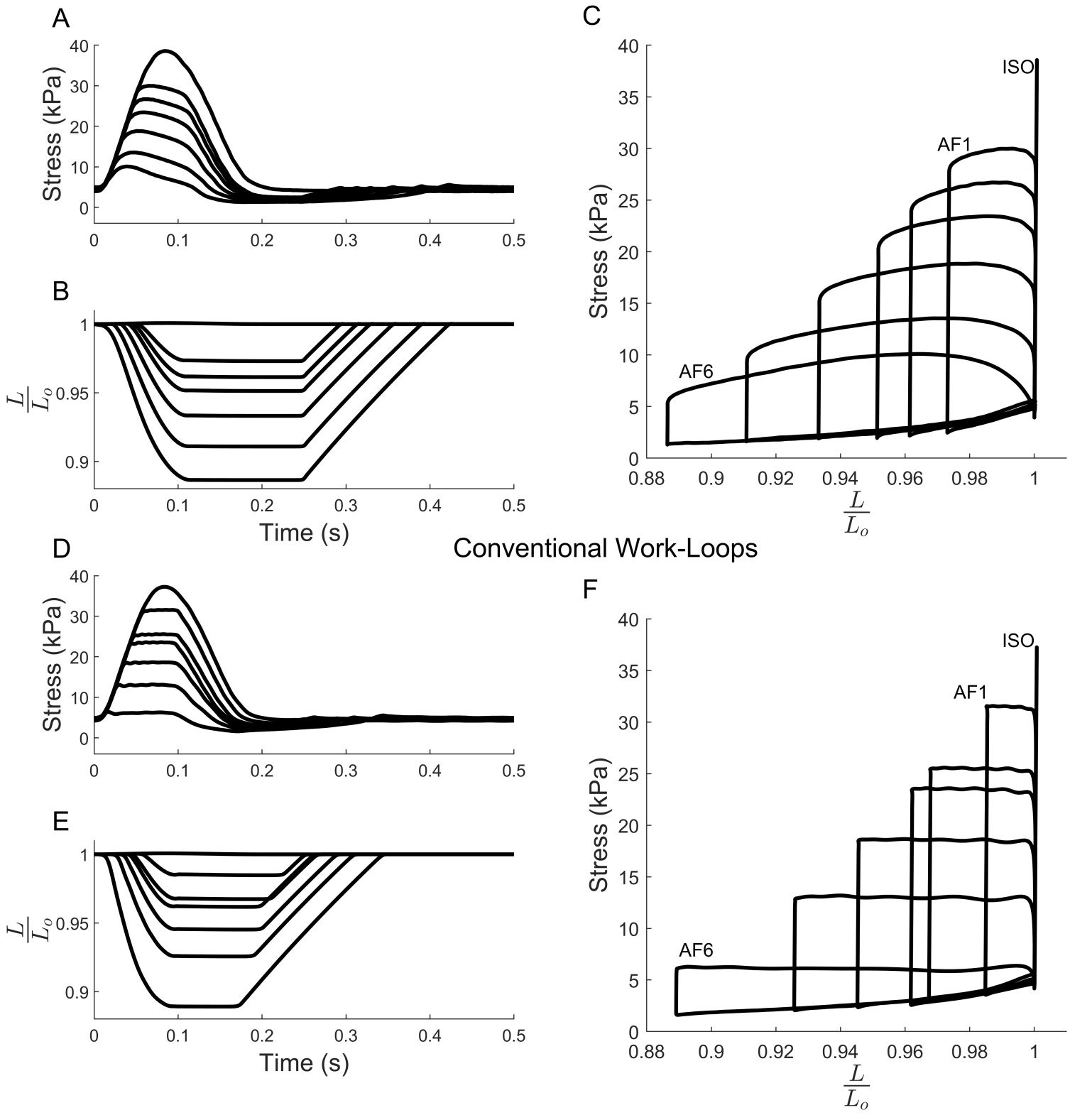

Downloaded from journals.physiology.org/journal/ajpheart at Univ of Auckland Lib (130.216.209.065) on August 2, 2022.

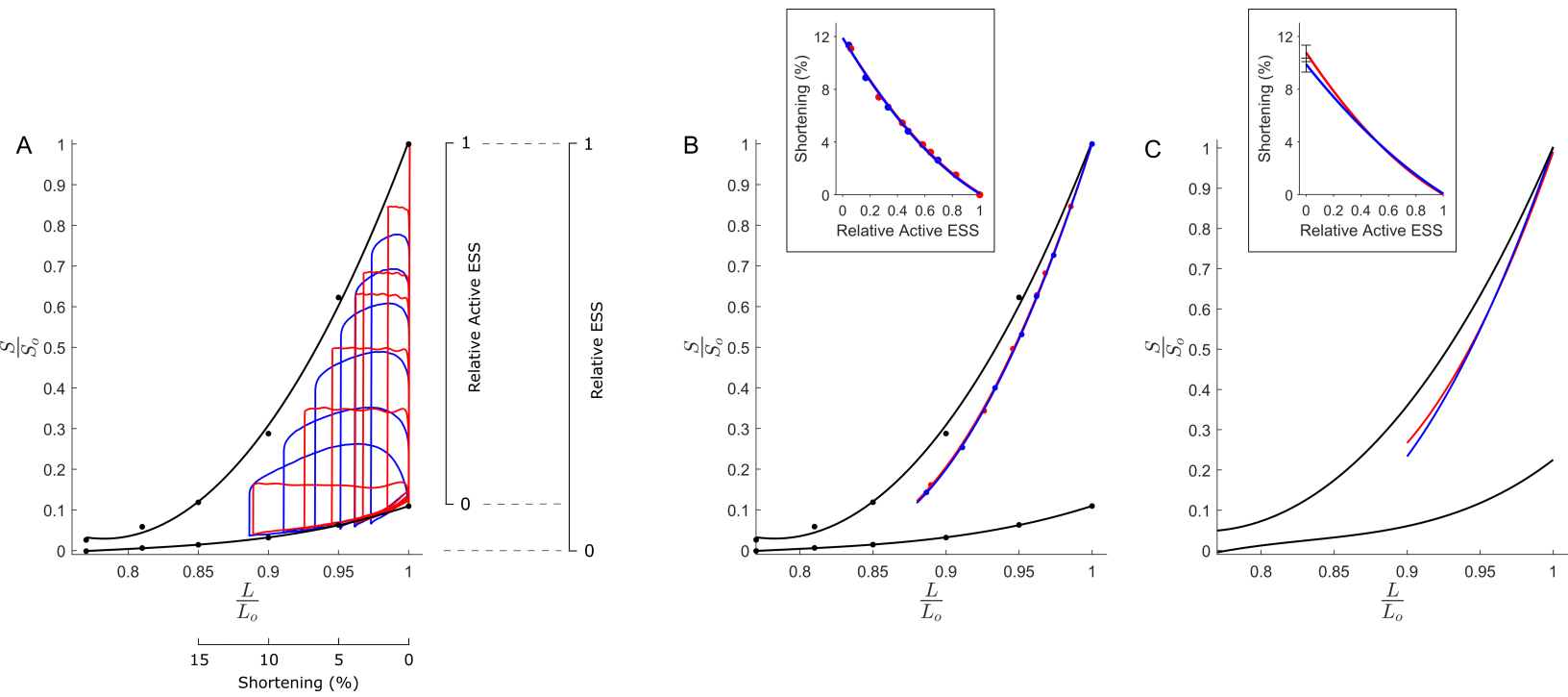

Downloaded from journals.physiology.org/journal/ajpheart at Univ of Auckland Lib (130.216.209.065) on August 2, 2022.

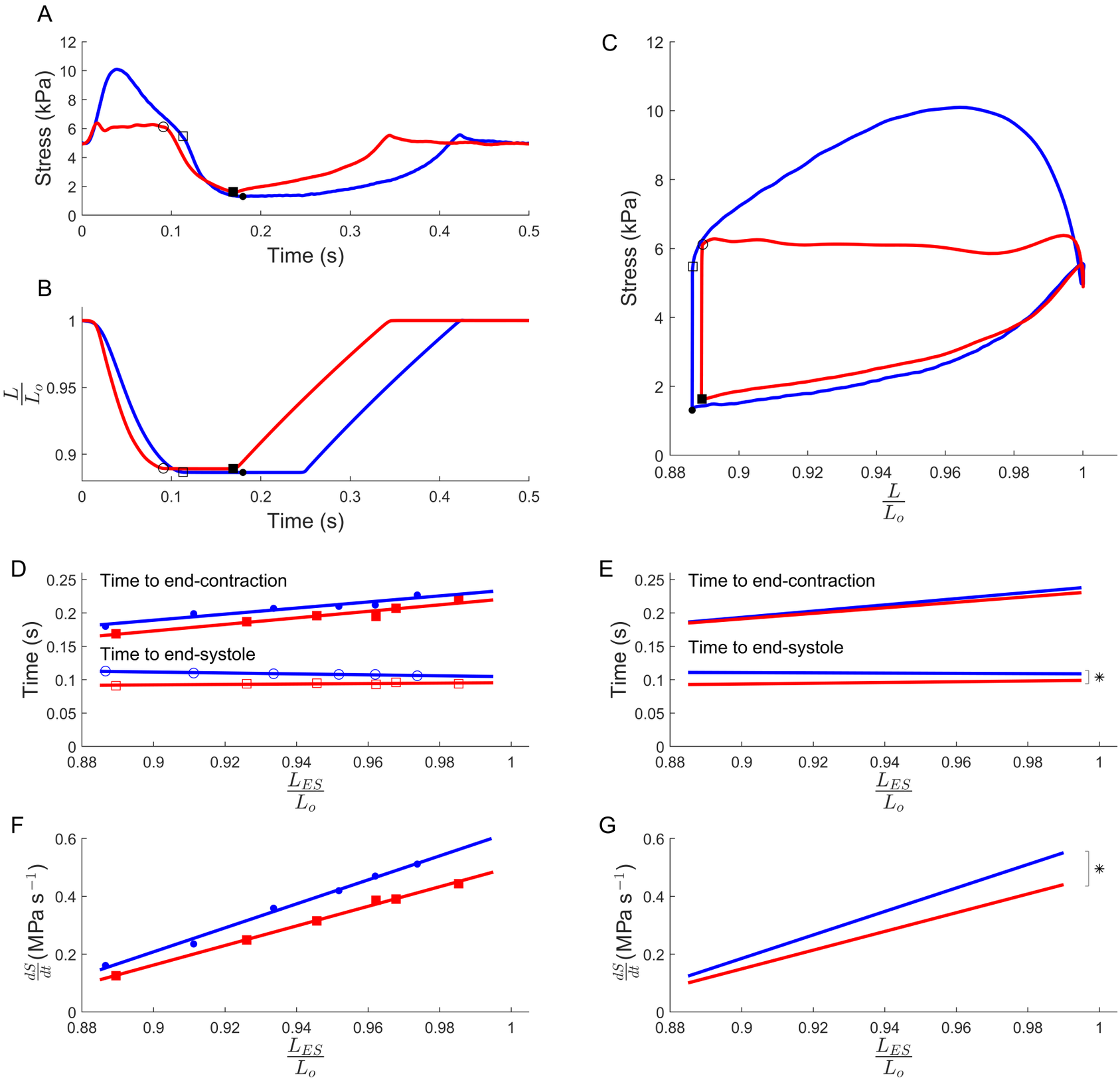

Downloaded from journals.physiology.org/journal/ajpheart at Univ of Auckland Lib (130.216.209.065) on August 2, 2022.

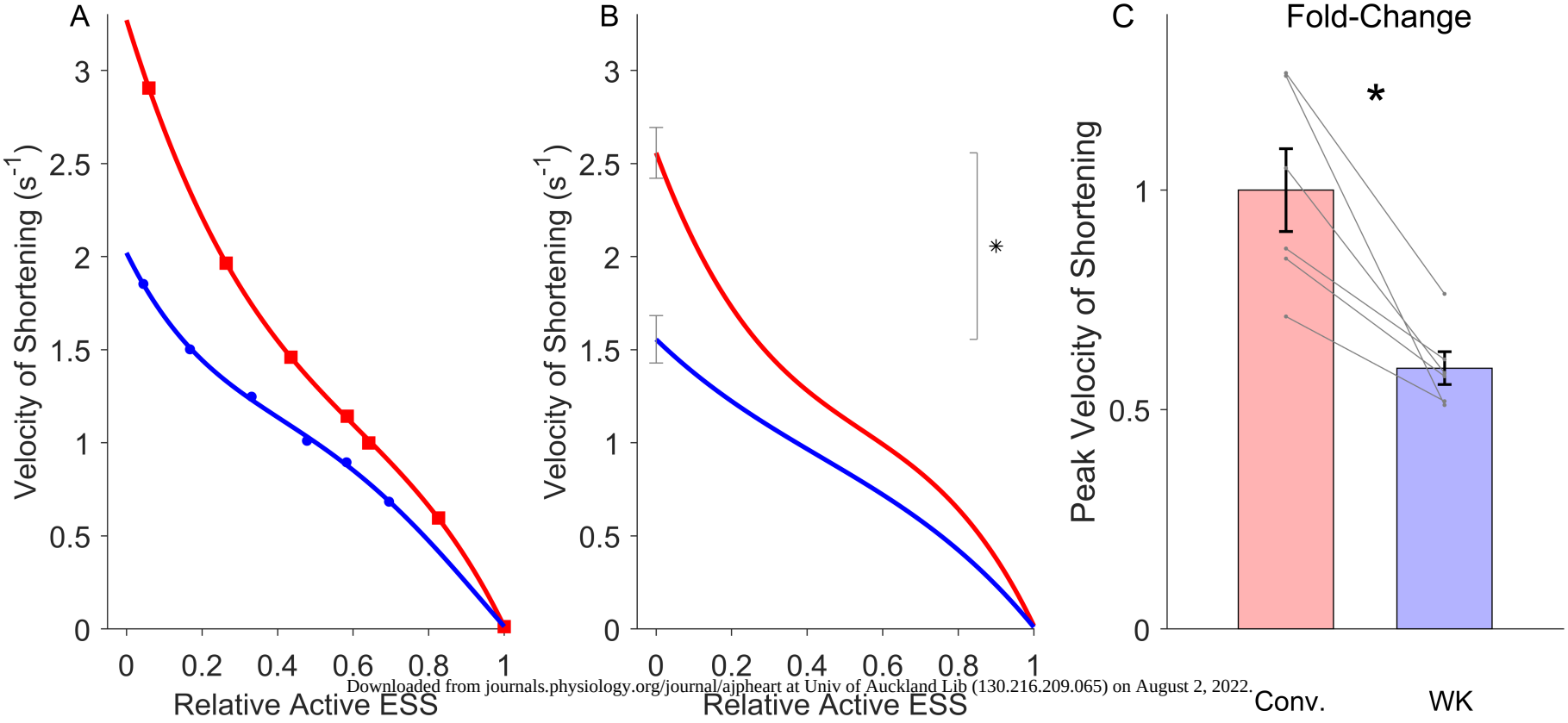

Downloaded from journals.physiology.org/journal/ajpheart at Univ of Auckland Lib (130.216.209.065) on August 2, 2022.

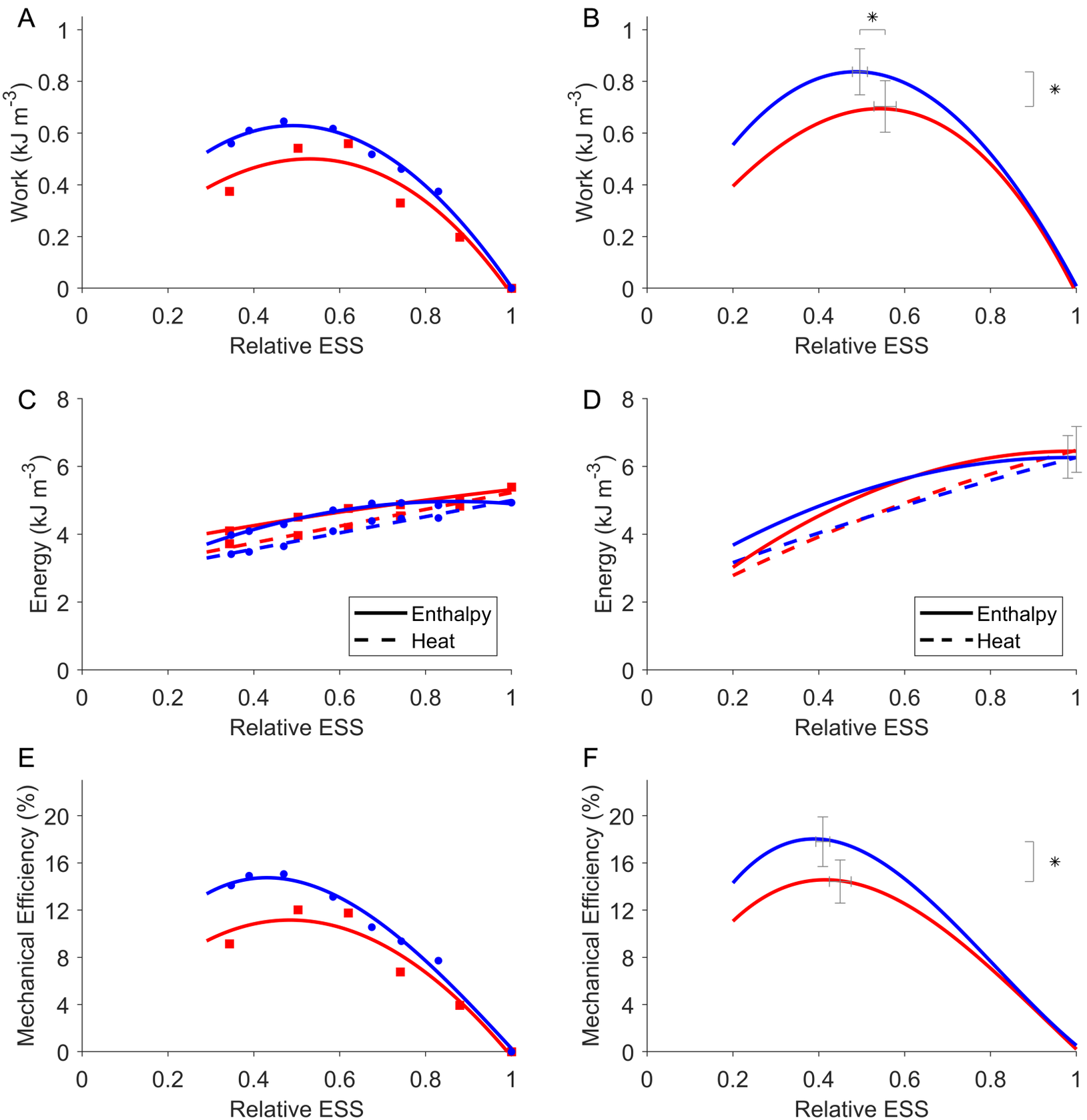

Downloaded from journals.physiology.org/journal/ajpheart at Univ of Auckland Lib (130.216.209.065) on August 2, 2022.

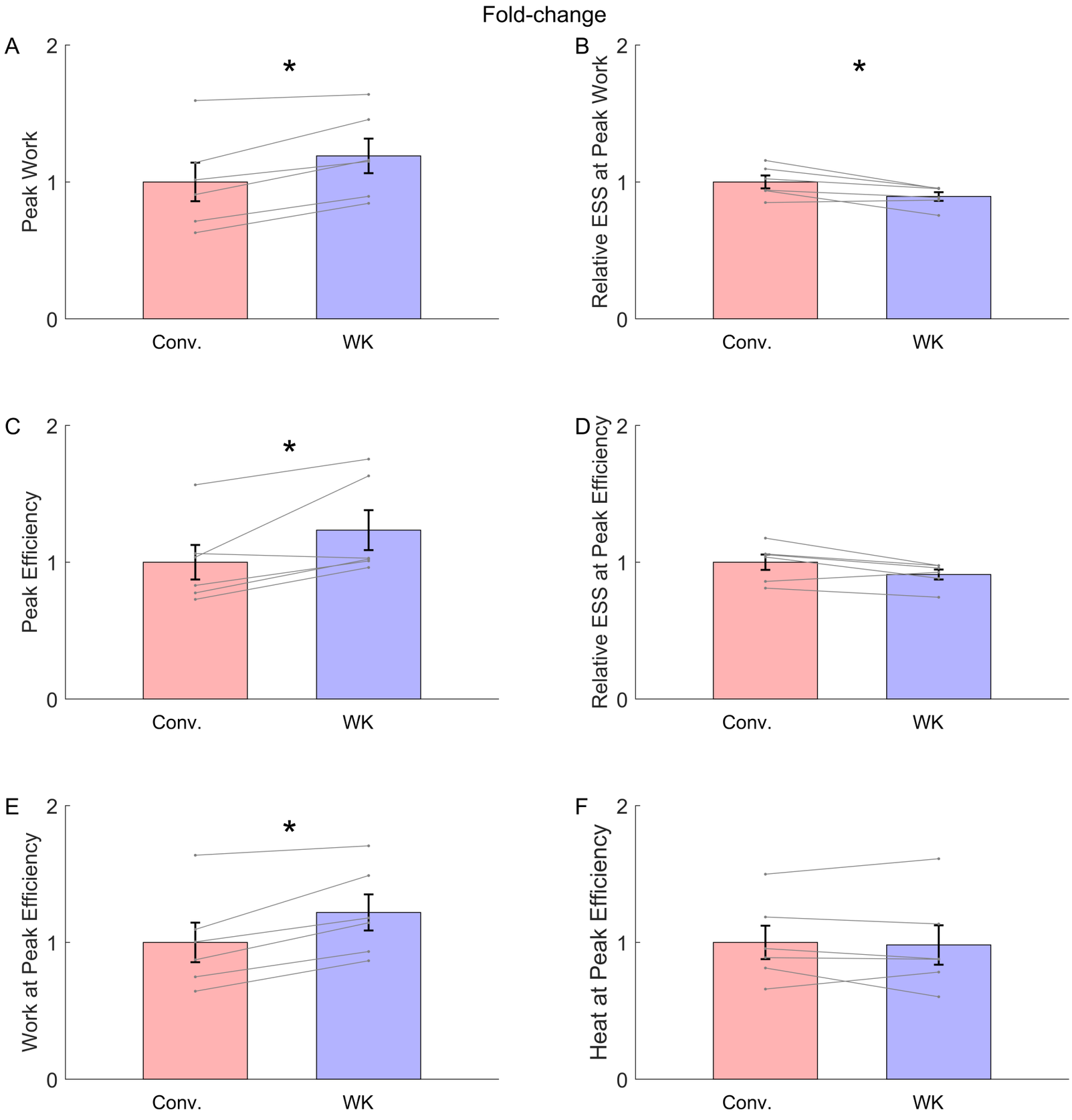

Downloaded from journals.physiology.org/journal/ajpheart at Univ of Auckland Lib (130.216.209.065) on August 2, 2022.

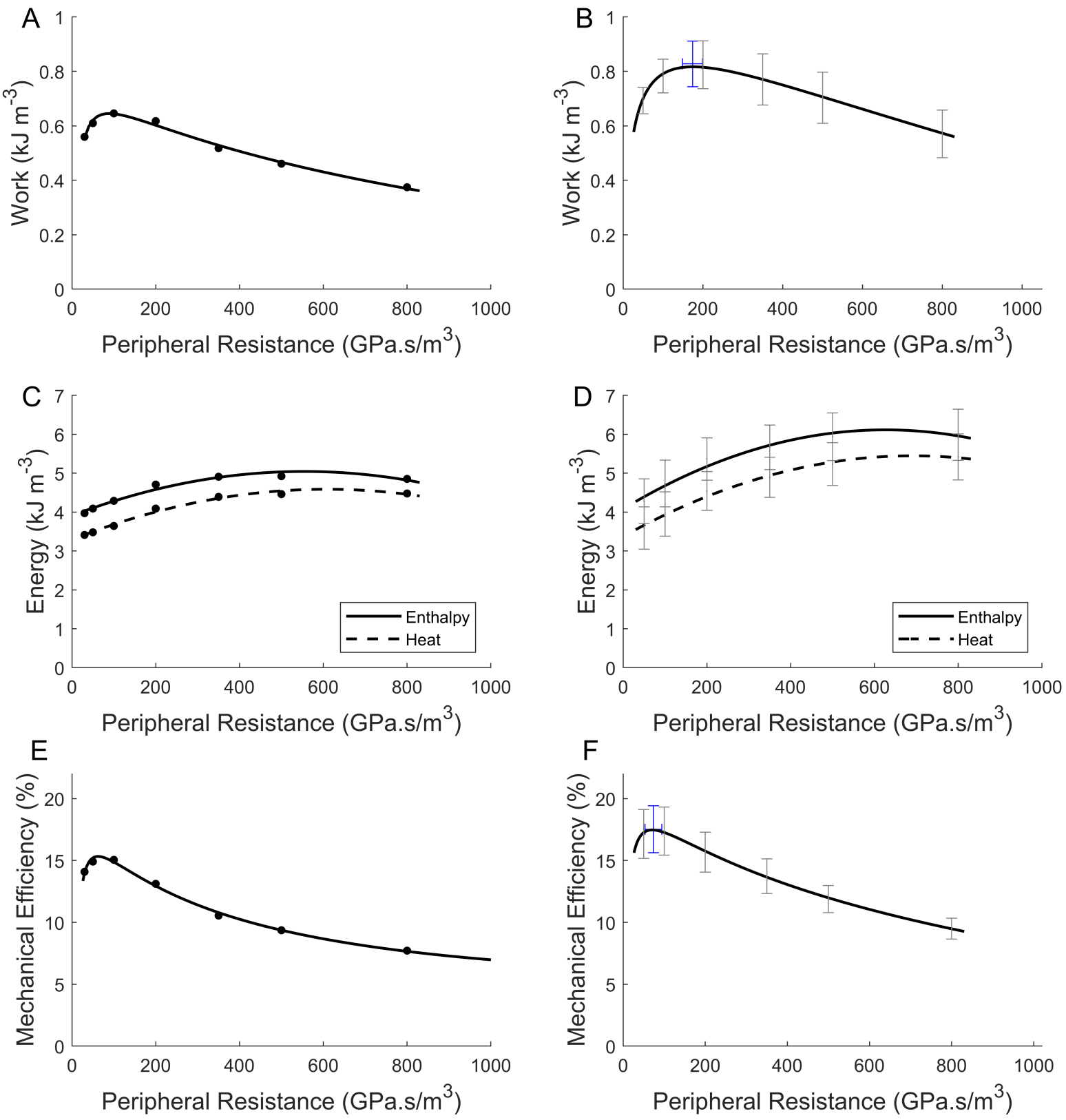

Downloaded from journals.physiology.org/journal/ajpheart at Univ of Auckland Lib (130.216.209.065) on August 2, 2022.